HOSTED BY
ELSEVIER
Available online at www.sciencedirect.com
ScienceDirect
Soils and Foundations 62 (2022) 101156
www.elsevier.com/locate/sandf

Technical Paper

Direct shear behavior of gravel-rubber mixtures: Discrete element modeling and microscopic investigations

Kevin Chew [a], Gabriele Chiaro [a,*], Jayan S. Vinod [b], Ali Tasalloti [a], Krishna Allulakshmi [b]

[a] Department of Civil and Natural Resources Engineering, University of Canterbury, Private Bag 4800, Christchurch 8140, New Zealand
[b] School of Civil, Mining and Environmental Engineering, University of Wollongong, Wollongong, NSW 2522, Australia

Received 18 September 2021; received in revised form 15 March 2022; accepted 20 April 2022

Abstract

In this paper, a newly developed 3-dimentional discrete element model (DEM) for gravel-rubber mixtures (GRMs), namely DEM4GRM, that is capable of accurately describing the macro-scale shear response (from small to large deformation) of GRMs in a direct shear box apparatus is presented. Rigid gravel grains are modelled as simple multi-shape clumps, while soft rubber particles are modeled by using deformable 35-ball body-centered-cubic clusters. Mixtures are prepared with different volumetric rubber content (VRC) at 0, 10, 25, 40 and 100%, statically compressed under 30, 60 and 100 kPa vertical stress and then sheared, by closely simulating a reference laboratory test procedure. The variation of micro-scale factors such as fabric, normal and tangential force anisotropy is carefully examined throughout the shearing process and described by means of novel micro-mechanical relationships valid for GRMs. Moreover, strong-force chains are scrutinized to identify the transition from rigid to soft granular skeleton and gain insights on the load transfer and deformation mechanisms of GRMs. It is shown that the development of the fabric and force anisotropy during shearing is closely related to the macro-scale shear strength of GRMs, and strongly depends on the VRC. Besides, strong-force chains appear to be primarily formed by gravel-gravel contacts (resulting in a rigid-like mechanical behavior) up to $VRC = 30\%$, and by rubber-rubber contacts (causing a soft-like mechanical response) beyond $VRC = 60\%$. Alternatively, at $30\% < VRC < 60\%$, gravel-rubber contacts are predominant in the strong-force network and an intermediate mechanical behavior is observed. This is consistent with the behavioral trends observed in the macro- and micro-mechanical responses.

Keywords: Discrete element method; Direct shear; Gravel-rubber mixtures; Deformable rubber particles; Fabric and force anisotropy; Strong-force chains

1. Introduction

End-of-life tires (ELTs) are waste scrap tires that no longer can be used for their original purpose. Currently, in New Zealand, ETLs are produced at an annual rate of 6.3 million (Tyrewise, 2020), and 70% of such ETLs are disposed in landfills, stockpiles or unaccounted for (Ministry for the Environment, 2015). Their effective reuse and recycling through large-scale civil engineering projects is a national priority. It will minimize land usage for stockpiling and potential soil and groundwater contamination, reduce disposal costs, lessen the risk of toxic tire fires, and preserve natural resources (Chiaro et al., 2020).

Aimed at providing a sustainable engineering solution to the ELT disposal in New Zealand, the authors have conducted a feasibility study on the use of ELT-derived aggregates (in the form of granulated rubber) blended with gravelly soils as an effective energy-absorption layer for geotechnical seismic-isolation (GSI) with energy dissipation foundation systems for low-rise light-weight residen-

Peer review under responsibility of The Japanese Geotechnical Society.
* Corresponding author.
E-mail address: gabriele.chiaro@canterbury.ac.nz (G. Chiaro).

https://doi.org/10.1016/j.sandf.2022.101156
0038-0806/

tial buildings. Low-shear modulus and high damping materials such as sand-rubber mixtures (SRMs) have been previously proposed for use as GSI layers (Tsang, 2008, 2009; Tsang et al., 2012). However, the compressible nature of SRMs in the GSI layer leads to low bearing capacity and unacceptable high settlement of foundations (Dhanya et al., 2018, 2020). In view of this, a GSI system consisting of gravel-rubber mixtures (GRMs) has been proposed by the authors (Chiaro et al., 2019; Hernandez et al., 2020). Similar recommendations have been made also by Tsang et al. (2021) and Pitilakis et al. (2021).

As described in Tasalloti et al. (2020, 2021a, 2021c), Chiaro et al. (2021) and Banasiak et al. (2021), the authors have carried out comprehensive geo-environmental laboratory investigations on a variety of GRMs to evaluate their geotechnical properties (i.e., specific gravity, compaction, shear strength, compressibility, small-strain shear stiffness, shear modulus degradation and damping ratio) and environmental characteristics (i.e., pH, hydraulic conductivity, total organic carbon and concentration of leachate chemical contaminants). GRMs having volumetric rubber content (*VRC*) up to 40% have adequate strength (friction angle $> 35°$), reduced compressibility and long-term settlement under sustained static load, high stiffness, and excellent energy absorption properties. Remarkably, when gravel-size like rubber particles are used in the mixtures, the leaching of toxic metal and chemical contaminants (e.g., zinc) is considerably minimized as compared to the case of sand-size like rubber particles.

The results of this investigation have provided very useful insights on the physical and macro-mechanical behavior of GRMs, well complementing limited existing studies reported in the literature (Anastasiadis et al., 2012; Senetakis et al., 2012; Pistolas et al., 2015; Pasha et al, 2019; Hazarika et al., 2020). Nevertheless, due to the heterogeneity of these granular synthetic materials (i.e. blends of rigid gravel grains and soft rubber particles), their ultimate adoption as engineered fills for GSI foundation applications, must be supported by an in-depth understanding of their macro- and micro-mechanical response as well as the transition from rigid to soft granular skeleton, which greatly influence the load transfer and deformation mechanisms of such uncommon materials.

Discrete Element Method (DEM) has been widely used as a tool to investigate particle-level interactions and develop a better understanding of the mechanical behavior of granular soils (e.g., Sitharam et al., 2002; Cui and O'Sullivan, 2006; Sitharam et al., 2009; O'Sullivan, 2011; Huang et al., 2014; Ngo et al., 2014; Indraratna et al., 2014; Ostubo and O'Sullivan 2018; Garcia and Bray, 2019; Gong et al., 2019a; Morimoto et al., 2021; among others). The granular and discrete nature of typical rigid soil-soft rubber mixtures makes DEM an ideal numerical modelling technique to investigate the micro-mechanical behavior of such materials (Lopera-Perez 2017a, 2017b; Asadi et al., 2018; Lopera-Perez et al., 2018; Zhang et al., 2020). However, the soft and low moduli behavior of the rubber particles challenges one of the fundamental assumptions of DEM: particle rigidity. Based on this assumption, contact forces are determined from the overlap between contacting bodies but the particles do not deform (O'Sullivan, 2011). While the softness of rubber may be captured by prescribing a low particle stiffness, the volumetric behavior of pure rubber (Poisson's ratio $\nu^{rubber} = 0.5$) cannot be replicated easily in DEM using the particle rigidity approach. Previous studies (e.g. Lopera-Perez et al., 2017; Wang et al., 2018) have modelled rubber particles as spheres or simple clump shapes with stiffness parameters typically defined using engineering properties of rubber or as a ratio of the rigid soil particle stiffness. Limited validation of the compressive volumetric behavior of the individual rubber particles has been provided or undertaken in such studies.

More recent studies have acknowledged the importance of modelling the rubber-like particle behavior in a more realistic way. For instance, Asadi et al. (2018) implemented a deformable agglomerate to model more accurate changes in the shape (deformation) of rubber particles. The key purpose for this approach was to account for the increase in contact area of the rubber particles during compression and shearing loading conditions. A deformable aggregate was created using weak internal bonds between tire rubber particles, allowing the spheres within a cluster to move and rearrange. Alternatively, Ren et al. (2020) proposed a deformable single rubber particle model, calibrated with respect to compression and tensile element tests, that is able to capture the volumetric behavior of rubber ($\nu^{rubber} = 0.5$). It has been recommended that with sufficient rows of bonded spheres packed in a body-centered cubic (BCC) arrangement, such a model can reliably and accurately capture the strength and volumetric behavior of a single rubber particle as the non-linear mechanical behavior of rubber is captured by a piecewise linear contact/bond model. Although the latter model is very promising, its application to reproduce the results of element tests involving assemblies of rubber particles has not been attempted yet, and impending computational implications arising from the simultaneous use of a large number of deformable BCC elements has not been addressed yet. This is attempted in this current study as described hereafter.

Physical grain-scale experiments (e.g., Paulick et al., 2015; Senetakis and Coop, 2014) have become a useful reference for better understanding particle-level behavior of granular materials and to support DEM studies. For example, Tian and Senetakis (2022) investigated sand-rubber contact interactions using a custom-built micro-mechanical apparatus and observed the importance of accounting for rubber particle deformation in the contact model. Such experiments also allow a direct measurement of contact and mechanical properties on studied material that can be used to define the input parameters for DEM models (Coetzee, 2017; González-Montellano et al., 2012).

Given the above background, and taking advantage of both the well-established particle rigidity approach applica-

ble to rigid gravel grains and the possibility to capture the soft rubber behavior using BCC deformable particles, in this paper, a discrete element approach is used to explore the particle-to-particle mechanisms responsible for the macro-scale small-to-large shear deformation behavior of GRMs. Specifically, a 3D hybrid DEM model for GRMs (DEM4GRM) is developed using the Particle Flow Code 3–Dimensional program (PFC3D, version 6.1; Itasca Consulting Group, 2018). Such model makes it possible to explore the micro-mechanical direct shear behavior of GRMs under varying *VRC* and normal stress levels. By calibrating the DEM4GRM model with experimental direct shear test results on GRMs and physical grain-scale compression tests on single rubber particles, reliable interpretation of micro-mechanical parameters could be made, yielding a methodological identification of gravel-like, intermediate and rubber-like behavioral zones as a function of *VRC*.

2. Experimentally observed direct shear behavior

To date, the authors have investigated the direct shear behavior of 6 types of GRMs (made by mixing angular and rounded gravels and three different granulated rubber particles sizes), as reported in detail in Tasalloti et al. (2020, 2021a, 2021c) and Chiaro et al. (2021). In this paper, only the results of a selected series of direct shear tests are briefly reported with the main purpose of supporting the numerical work described henceforward and providing the necessary experimental benchmark.

Testing materials consist of non-spherical (i.e. cubic-like) recycled granulated tire rubber particles (specific gravity $G_{s,R} = 1.15$; mean particle size $D_{50,R} = 3.7$ mm) and a uniformly-graded rounded gravel (specific gravity $G_{s,G} = 2.71$; $D_{50,G} = 5.6$ mm). The rubber is free from steel wires and fiber reinforcement. Particle size distribution curves alongside photographic images of the gravel and rubber used in this study are shown in Fig. 1. A summary of their index properties is reported in Table 1. By combining the two reference materials, mixtures are prepared with different volumetric rubber content (*VRC*) at 0, 10, 25, 40 and 100%, where *VRC* is defined by Eqn. (1):

$$VRC = \frac{V_{rubber}}{V_{gravel} + V_{rubber}} \quad (1)$$

A medium-size (100 × 100 × 53 mm – length × width × height) direct shear box apparatus is used to evaluate the stress–strain-volumetric behavior of the two reference materials (gravel and rubber) and their selected mixes. After thoroughly mixing gravel and rubber particles, uniform rigid-soft granular mixtures are attained by the dry tamping method. In the process, segregation is avoided by carefully placing the mixes in the testing apparatus, and gently tamping dry specimens until achieving 50% relative density (D_r), which is calculated based on

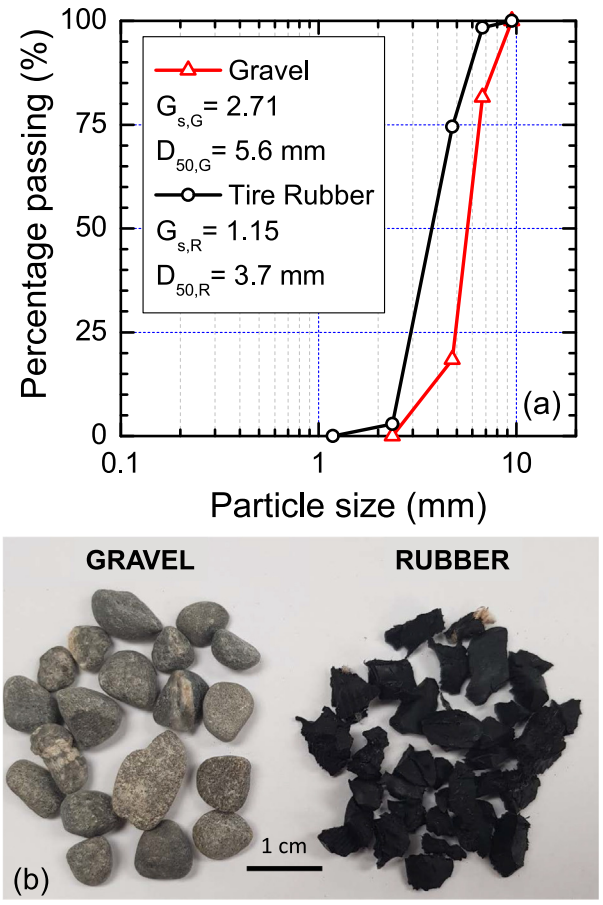

Fig. 1. Testing materials: (a) particle size distribution curves; and (b) photographic images.

the maximum void ratio (e_{max}) determined according to ASTM D4253-16, (2016), and the minimum void ratio (e_{min}) defined by standard Proctor compaction tests (ASTM D698-12, 2012). Dry GRM specimens are then compressed under 30, 60 and 100 kPa normal stress (σ_n), and subsequently sheared at horizontal displacement rate of 1 mm/min (ASTM D3080-11, 2011).

Under the direct shear conditions considered in this study, the mechanical behavior of GRMs is *VRC* and stress level (σ_n) dependent. Typical shear stress-horizontal displacement relationships and volumetric responses observed for GRMs are shown in Fig. 2(a)–(f). At $VRC \leq 25\%$, GRMs specimens show a gravel-like dilative response (i.e. increase in volume) with a well-defined peak shear stress followed by strain softening. Alternatively, at higher *VRC*, GRMs exhibit a rubber-like contractive behavior (i.e. decrease in volume) beside strain hardening without an apparent peak strength state. Such behavioral trends are essentially similar across the three level of σ_n applied; however, the higher is σ_n, the stiffer is the initial response of each material as well as their maximum shear strength. Similar macro-mechanical response for GRMs was observed by Pasha et al. (2019) in drained triaxial tests.

Table 1
Index properties of gravel-rubber mixtures tested in this study.

Mixture ID	Volumetric rubber content, *VRC* (%)	Specific gravity, G_s	Maximum void ratio, e_{max}	Minimum void ratio, e_{min}	Initial void ratio, e_0 *
G100-R0	0	2.71	0.725	0.545	0.63
G90-R10	10	2.51	0.778	0.561	0.65
G75-R25	25	2.33	0.818	0.577	0.70
G60-R40	40	2.09	0.912	0.590	0.74
G0-R100	100	1.15	1.272	0.787	1.01

* Corresponding to 50% relative density before the application of 30, 60 and 100 kPa normal stress (i.e. 1-D compression) in the direct shear tests.

3. GRM discrete element modeling

3.1. Proposed DEM model for GRMs

The numerical framework in PFC3D is based on the DEM formulation by Cundall and Strack (1979), where an explicit numerical scheme is used to monitor the interaction of particles individually and its corresponding contacts with neighboring particle. Moreover, based on the aforementioned particle rigidity approach, contact forces are evaluated from the overlap between contacting bodies but the particles do not deform (O'Sullivan, 2011).

Specifically, in this study, the Hertz-Mindlin contact law (Mindlin and Deresiewicz, 1953) was used to define the interactions at each contact. This contact model follows a non-linear contact force-overlap relationship governed by the user-defined initial shear modulus (G) and a dashpot component for damping. The DEM input parameters defining the contacts are provided in Table 2. As the gravel and rubber particles have different engineering properties, the inheritance of surface properties (available in PFC3D) is used to determine hybrid contact properties between the gravel and rubber particles (Itasca, 2018). The shear modulus (G) and Poisson's ratio (ν) of contacting individual gravel and rubber particles is computed as follows:

$$G = 2G^*(2-\nu) \tag{2}$$

$$\nu = \frac{4G^* - E^*}{2G^* - E^*} \tag{3}$$

where

$$E^* = \left(\frac{1-\nu^{gravel}}{2G^{gravel}} + \frac{1-\nu^{rubber}}{2G^{rubber}}\right)^{-1} \tag{4}$$

$$G^* = \left(\frac{2-\nu^{gravel}}{G^{gravel}} + \frac{2-\nu^{rubber}}{G^{rubber}}\right)^{-1} \tag{5}$$

It is important to mention that the friction coefficient at the gravel-rubber contact is taken as the minimum of the two particles (Itasca, 2018).

Particle shape plays an important role in DEM modelling. The accuracy to which particle shape are replicated is often a balance between the number of particles, computational cost, and number of input parameters required. Simple spheres, whilst computationally efficient, required modification to its contact laws (e.g., rolling friction) to imitate the effects of particle shape and asperities in order to produce accurate results. Thus, increasing the number of input parameters and calibration steps required. In this study, clumps are used instead of spheres to account for particle shape effects, which can significantly influence packing, shear strength and volumetric behavior of the DEM specimens (Coetzee, 2017).

3.1.1. DEM modelling of single tire rubber particles

Recognizing the importance of accounting for the compressive volumetric behavior of rubber, an improved tire rubber particle model is used in the DEM4GRM, which builds on the findings from Asadi et al. (2018) and Ren et al. (2020). Specifically, to limit the number of particles required to achieve a realistic simulation setup and reduced computation time, the BCC rubber model by Ren et al. (2020) is enhanced and optimized. Fig. 3 shows the proposed 35-ball-BCC rubber model consisting of a cluster of 35 balls, BCC packed, bonded together by linear parallel bonds (Potyondy and Cundall, 2004). The inter-cluster non-bond contacts, which would form when in contact with external particles, are defined using the Hertz-Mindlin model (Mindlin and Deresiewicz, 1953). To ensure that compressive load is applied more evenly, an outer shell/row of particles surrounds the 9-particle cubic core (internal cube structure), providing sufficient degrees of freedom for a 3D volumetric response.

The compressive mechanism of the proposed 35-ball-BCC model is schematically illustrated in Fig. 4:

- *Stage 1*: when a single rubber particle is first synthesized in DEM4GRM, the internal linear parallel bonds hold the spheres (balls) together in the cluster, and the bonds form a BCC crystal lattice structure;
- *Stage 2*: once the particle is in contact with the walls, Hertzian contacts are formed at the contact points. As the particle is compressed, it behaves predominantly linearly as most of the deformation occurs in the (linear) internal bonds. This process also brings the spheres (balls) in the cluster closer together;
- *Stage 3*: when the intra-particles are in contact, Hertzian contacts eventually form. The combination of these intra-particle Hertzian contacts and the (linear) internal bonds gives rise to a non-linear compressive response of the particle at larger deformation level. Thus, allowing the rubber model to capture the characteristic non-linear load–displacement response of rubber.

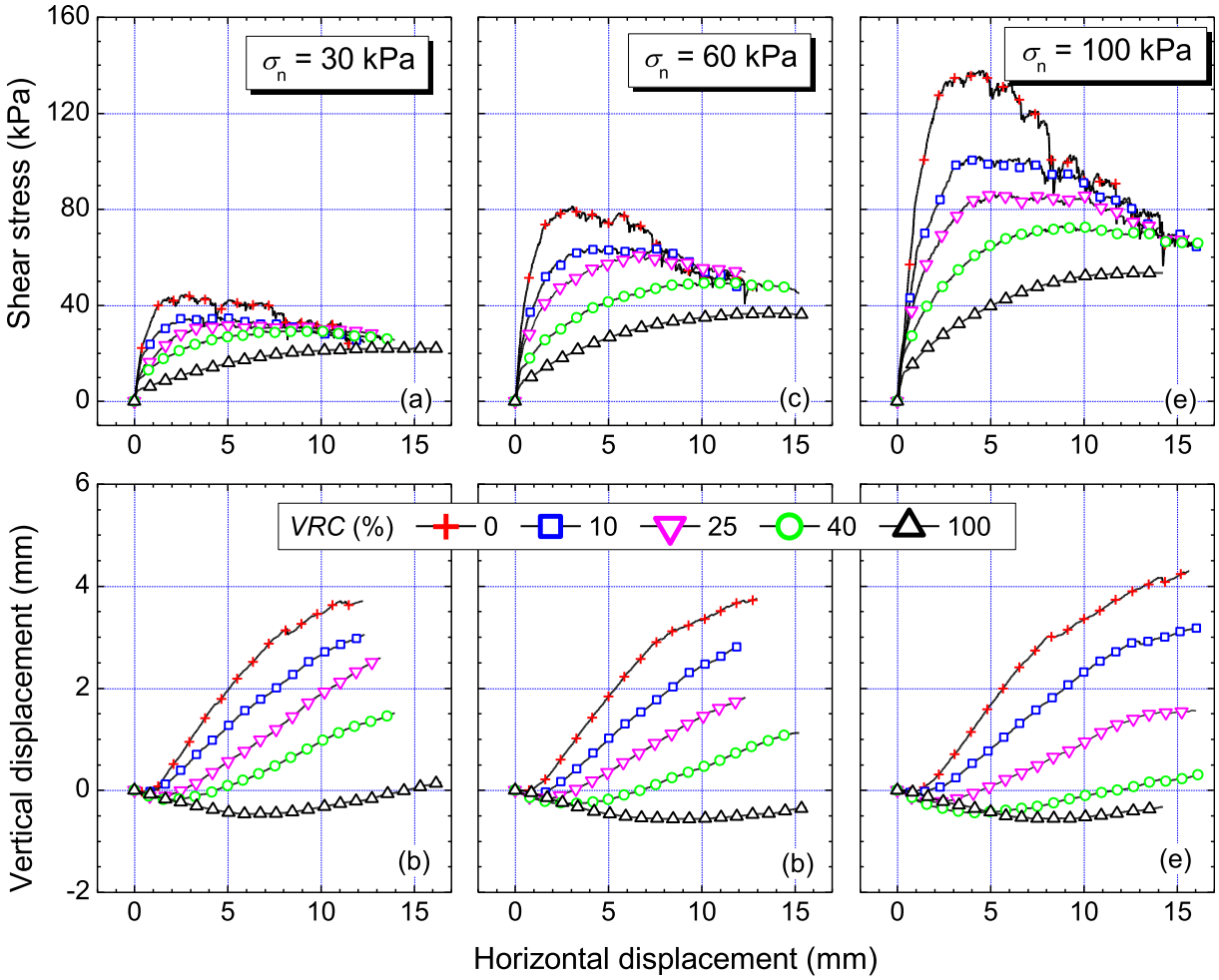

Fig. 2. Direct shear behavior of GRMs at 30, 60 and 100 kPa normal stress.

The proposed 35-ball-BCC rubber model introduces internal voids, which do not exist in reality. As a result, the mass of a DEM rubber particles would be underestimated should the same density of 1150 kg/m^3 (Tasalloti et al., 2020) as measured in the laboratory be considered. As illustrated in Fig. 5, a greater particle density is, therefore, assigned to the DEM particles to account for the presence of these voids. It is estimated that a 35-ball-BCC rubber particle occupies approximately 72% of the equivalent solid volume rubber particles, and the corrected density of rubber is therefore found to be 1610 kg/m^3. A detailed mathematical derivation has been presented by Chew (2021).

A series of physical grain-scale uniaxial compression tests on single tire rubber particles is carried out in this study to experimentally calibrate the 35-ball BCC rubber model (Fig. 6a). Non-linear load–displacement trends are identified. The slight variation in the relationships shown in Fig. 6(b), is primarily due to the irregular shape and difference in size of tested rubber particles (refer to Fig. 1b). Subsequently, in the DEM model, a typical 35-ball-BCC rubber particle is compressed by mimicking the actual experimental set up (Fig. 6c). The DEM load–displacement response is determined by measuring the load from the reaction force at the wall and the vertical displacement of the top wall. The transition from linear to non-linear response is clearly shown in the load–displacement response of the tire rubber model (Fig. 6d), showing a close match in the compressive response of the tire particle between the experimental test and DEM simulation results. The best combination of Hertzian shear modulus (G) and Linear Parallel Bond's elastic modulus (E) that approximate the non-linear load–displacement response is obtained through a process of trial and error. The calibrated model parameters are summarized in Table 2.

The volumetric behavior of the rubber cluster can be controlled by varying the normal-to-shear stiffness ratio (k_n/k_s) (Ren et al., 2020). By monitoring the displacement of the eight particles forming the *internal cube structure* under compression (Fig. 7a, b), the Poisson's ratio (v) is evaluated. Specifically, by considering the particle displacement and corresponding strains of the internal cube structure, v is estimated as indicated in Eqn. (6):

$$v = \frac{D_0 - D_i}{D_0} \cdot \frac{L_0}{L_0 - L_i} \tag{6}$$

Table 2
Input parameters and material properties for the DEM model.

Particle Type	Parameter	Value
Gravel	Particle Density (kg/m^3)	2710
	Coefficient of Friction	0.72
	Shear Modulus (MPa)	90
	Poisson's Ratio	0.3
Rubber	Particle Density (kg/m^3)	1610*
	Coefficient of Friction	0.27
Rubber - bonds	Shear Modulus of Bonded Spheres (MPa)	12
	Bond elastic modulus (MPa)	20
	Normal-to-shear stiffness ratio	4.0
	Tensile Strength (Pa)	30E200#
	Shear Strength (Pa)	30E200#
	Critical damping ratio	0.25
Wall	Coefficient of Friction	0.70
	Shear Modulus (MPa)	80,000
	Poisson's Ratio	0.25
Global	Damping Coefficient	0.2

* Corrected rubber density (refer to Fig. 5).
# Tensile and shear strength values are set very high to avoid any breakages of the bond within rubber particles.

where D is the transverse length and L is the length of the sides of the internal cube in the direction of loading (Ren et al., 2020).

Through a series of simulations, it is found that $k_n/k_s = 4.0$ yields a Poisson's ratio of approximately 0.5 (typical of pure rubber), as illustrated in Fig. 7(b).

3.1.2. DEM modelling of gravel particles

Gravel particles are modelled using simple clump shapes as those considered by Garcia and Bray, (2019). Although the clumps particles may have slightly more asperities, they provide a good approximation to the typical shapes of the gravel grains as illustrated in Fig. 8(a). It is worth noting that these asperities may be reduced by increasing the number of particles within a clump. However, this will significantly increase the computation time due to the increased number of particles required to replicate a smooth surface and the number of contacts that may form between particles.

A sieve analysis was simulated in PFC3D to validate the particle size distribution of the gravel clump assemblies generated in the model (refer to Chew, (2021) for details of the simulation setup). As shown in Fig. 8(b), the particle size distribution of the generated DEM gravel specimens is found to closely approximate that attained by physical sieve analyses.

3.1.3. DEM modelling of gravel-rubber mixtures

GRM specimens are generated using the overlapping method (Zhang et al., 2019) based on the particle size distribution from the laboratory experiments shown in Fig. 1 (a). The minimum and maximum void ratios are first determined by compressing the samples at 90% of the target normal stress while using friction coefficients of 0.0 and 2.0, respectively (Garcia and Bray, 2019). An iterative procedure is then used to determine a suitable friction coefficient that will produced a specimen of 50% relative density. The specimens are then quasi-statically compressed to the target void ratio representing 50% relative density. Confining pressure is applied on the specimen by loading the top plate as per the laboratory procedure. This methodology is applied instead of matching the experimen-

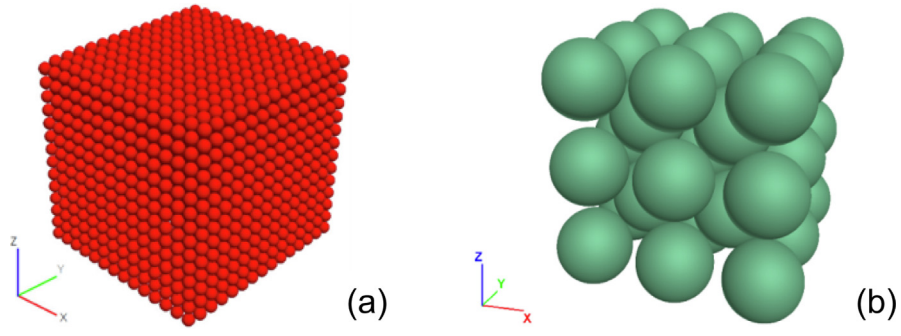

Fig. 3. Deformable single rubber particles used in DEM simulations: (a) Original BCC rubber model (Ren et al., 2020); and (b) 35-ball-BCC rubber model (this study).

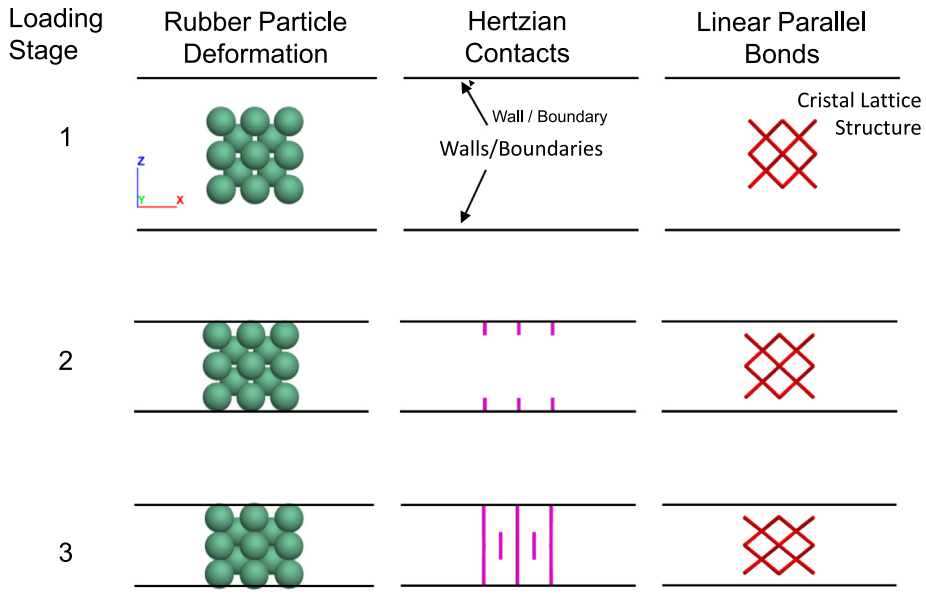

Fig. 4. Compressive mechanism implemented in the DEM4GRM model for 35-ball-BCC rubber particles.

tally determined initial void ratio in Table 1 to minimize the effects of any discrepancies in particle size, distribution, shape and asperity between the physical state and DEM model on the packing density (Salot et al., 2009). The void ratio values (evaluated at the end of compression and before shearing) for the different specimens considered in this study, and the number of particles used to generate the specimens, are summarized in Table 3, for completeness. In is important to note that, the differences in the void ratio values between the experiment (Table 1) and DEM study (Table 3) can be primarily attributed to the fact that the experimentally determined values do not account for the initial compression of the specimen post application of the confining pressure (Chew, 2021).

With the generation process complete, the particles are then assigned the friction coefficients defined in Table 2. To simulate a direct shear test, the assembly is sheared by moving the lower box at a displacement rate of 0.002 m/s. This rate was determined by limiting the inertia number, $I < 1E-4$ to maintain quasi-static conditions (Lopera-Perez et al., 2016). The inertia number is defined as $I = \dot{\varepsilon} D_{ave} \sqrt{(\rho/\sigma')}$, where $\dot{\varepsilon}$ is the strain rate, D_{ave} is the average particle size, ρ is the particle density and σ' is the mean effective stress assumed to be the normal stress applied in this study. The shear stress is measured along the wall boundaries (Indraratna et al., 2014; Gong et al., 2019b). Frictionless lateral walls are considered to allow for more realistic k_0 effects. Gravity is not applied throughout the simulation. Fig. 9 shows typical GRM specimens, including $VRC = 70\%$, which although not tested in the laboratory, it is tested in the DEM4GRM model to reveal trends at high rubber contents.

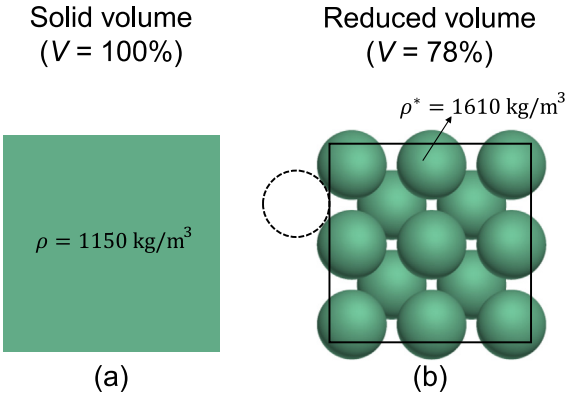

Fig. 5. Rubber density correction for internal voids: (a) reference solid-volume rubber particle; and (b) equivalent-density 35-ball-BCC rubber particle with internal voids. The black solid line represents the effective size/volume considered in the density correction.

The model parameters for the reference materials are determined by simulating the gravel ($VRC = 0\%$) and rubber ($VRC = 100\%$) behaviors in direct shear box tests and fitting the shear and volumetric response that best match the experimental results (Fig. 10) – training set. No additional model parameters are defined for mixtures with $VRC = 10$, 25, 40 and 70% (prediction set), but rather the shear and volumetric trends in the simulations are merely defined by the proportion of gravel and rubber particles in the mixtures and the normal stress level applied on the specimens. The calibrated model parameters are summarized in Table 2, and their selection is discussed below.

Gravel ($VRC = 0\%$): The Hertz-Mindlin model was adopted for the gravel particles to be consistent with the rubber particles and it is found to provide better match with the experimental results as compared to the linear contact model, especially across different stress levels. Moreover, the recent study by Tian et al. (2021) have shown that the Hertz contact model provides a good approximation to experimentally observed behaviors of

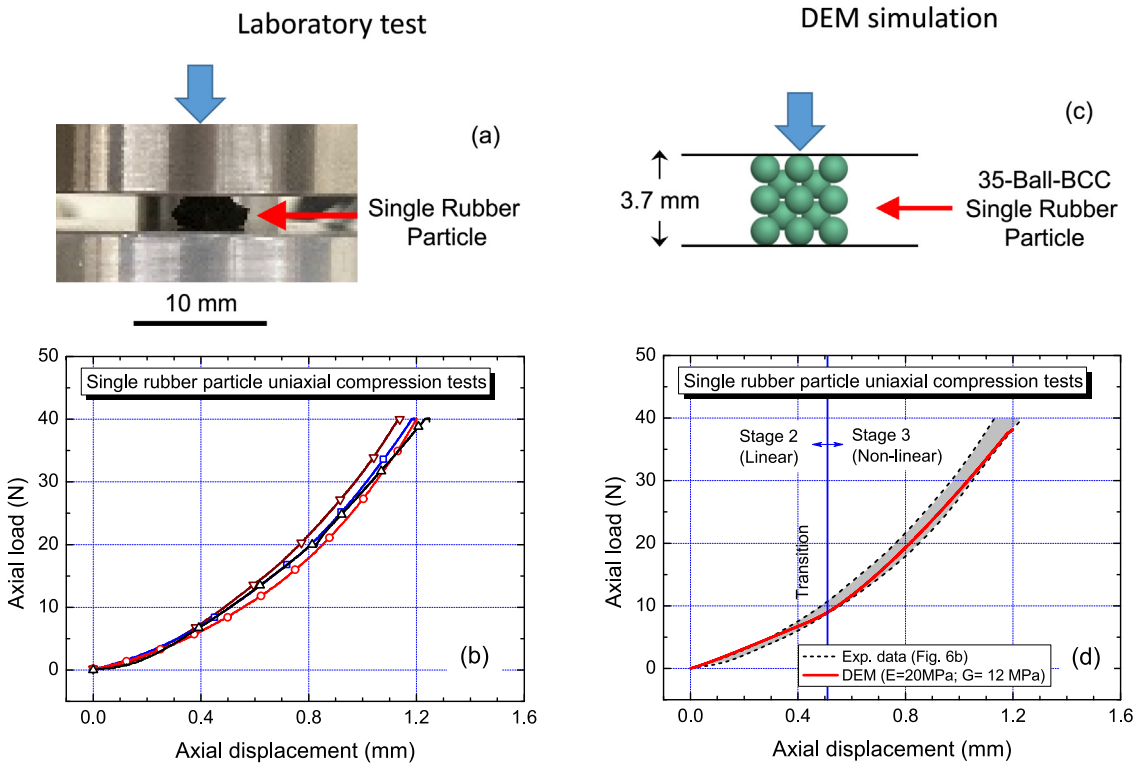

Fig. 6. Uniaxial compression response of single rubber particles: (a) experimental test setup; (b) experimental test results; (c) 35-ball-BCC model; and (d) DEM simulation results.

soft-rigid particles interacting on a grain-to-grain level. The calibrated shear modulus and friction coefficient of the gravel particles are found to be consistent with the experimentally derived bulk properties (Tasalloti et al., 2021a).

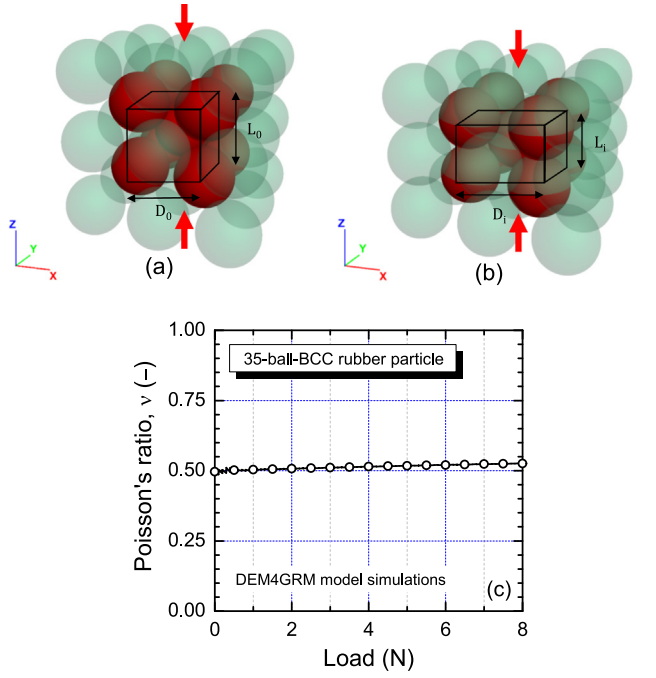

Fig. 7. Typical compression response of 35-ball-BCC single rubber particles: (a) zero volumetric deformation before load application; (b) volumetric deformation under applied load; and (c) measured Poisson's ratio at different load levels.

Rubber ($VRC = 100\%$): The stiffness parameters derived from the uniaxial compression tests in Fig. 6 are adopted in the direct shear test model. The friction coefficient of the rubber particles is varied to obtain the best fit with the experimental direct shear results. The selected friction coefficient of 0.27 is found to be lower compared to similar studies using sand-rubber mixtures (e.g. Evans and Valdes, 2008). This could be explained by the uneven surfaces of the 35-ball-BCC rubber particle used in this study where intra-particles can interlock with the surface gaps as illustrated in Fig. 5(b). Therefore, a lower interface friction coefficient is needed to offset the effects of this surface roughness.

4. DEM simulation results and discussions

4.1. GRM macro-mechanical response

Fig. 11 compares the relationships between the experimental test and DEM4GRM model simulation results for VRC = 10, 25 and 40% at 30, 60 and 100 kPa normal stress.

Such materials are essentially gravel-matrix dominated mixtures (refer to section 4.2 – behavioural zones for GRMs and Fig. 18 for details). Hence, alike the pure gravel specimens (Figs. 2 and 10), they display a stiff gravel-like behavior characterized by a clear peak followed by

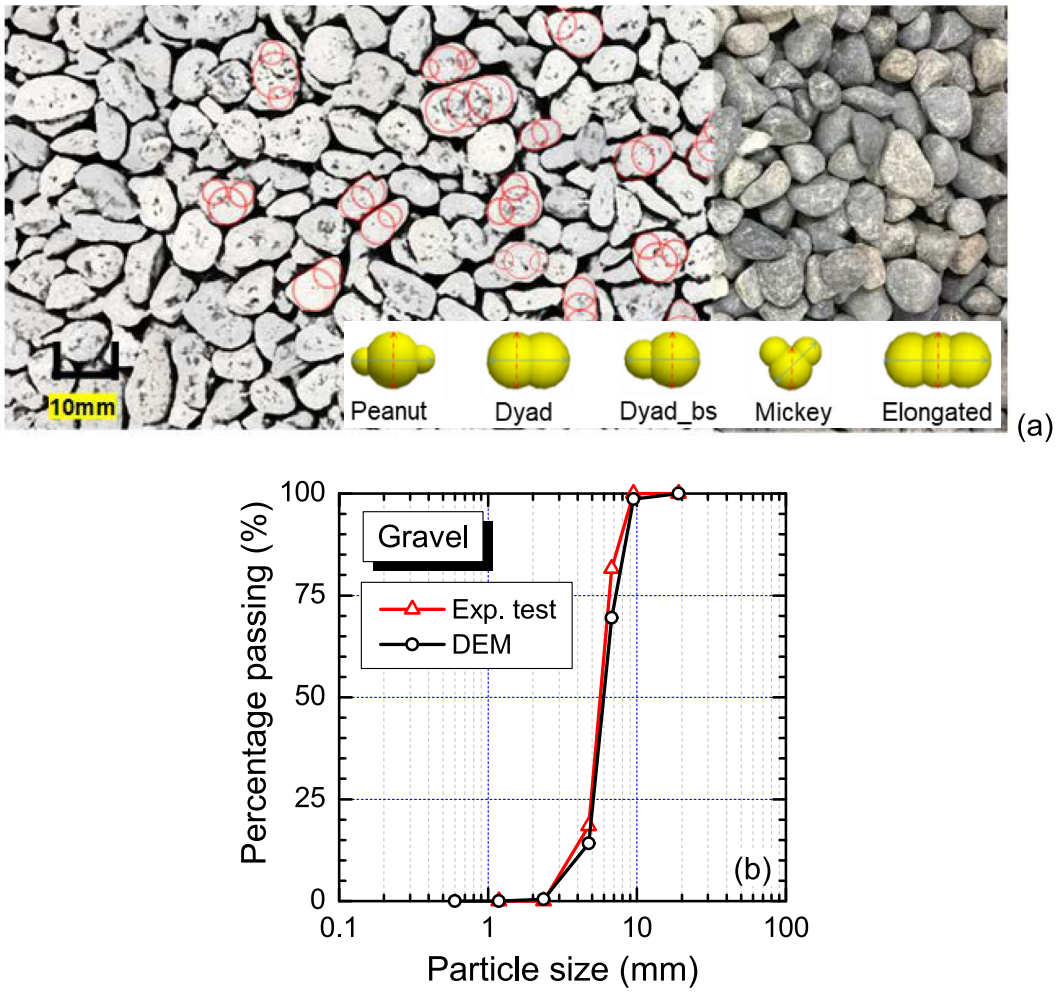

Fig. 8. Gravel clump assembly: (a) clumps shapes used in this study to model gravel particles; b) comparison between particle size distributions from experimental and DEM sieve analyses.

strain-softening, and accompanied by an increase in volume. Yet, as expected, as the rubber content increases in the mixtures, the initial stiffness, peak shear strength and residual shear strength decrease while a less dilative volumetric behavior is observed.

From a macro-mechanical viewpoint, it is observed that by increasing the normal stress, the peak shear stress (i.e. shear strength) increases, which is mainly due to the higher interlocking between particles as a result of higher normal stress applied on the specimens. In addition, a larger horizontal displacement is required to achieve the peak shear stress state. Moreover, looking at the vertical displacement during shearing, at lower normal stress a greater volumetric increase (i.e. dilation) is observed because particles can roll over each other as less particle deformation associated with rubber takes place. However, at higher normal stress, the amount of dilation is suppressed and more contraction is observed. This is mainly due to the high deformability of rubber particles. Eventually, at elevated normal stress of 100 kPa, the rigid grains of gravel are able to compress and deform the soft particles of rubber leading to a more contractive behavior (Tasalloti et al., 2021a, 2021b).

Overall, irrespective of the normal stress level and *VRC*, the DEM and the experimental shear stress-horizontal displacement responses are in very good agreement (Fig. 11a, c, e), in terms of initial stiffness, peak shear stress state and large-strain residual strength.

Contrarily, in the case of volumetric response (Fig. 11b, d, f), the agreement between DEM and experimental results is qualitatively correct (i.e., the numerical trends are consistent with the laboratory test results, in that increasing *VRC* results in a reduced dilative behavior), but quantitatively slightly dissimilar (i.e. the DEM model predictions somewhat overestimate the vertical displacement). Admittedly, such volumetric response predictions can be conveniently improved by choosing specific calibration factors for each individual *VRC* and stress level, but that would defeat the advantage of having limited model parameters and consistent information from a micro-mechanics viewpoint. Moreover, it would require a very time-consuming fitting process (i.e., the average computational time of the DEM simulations reported in this paper is 10 h). Therefore, this is not attempted in this study.

Table 3
Number of particles used in the DEM simulations conducted in this study.

Volumetric rubber content, *VRC* (%)	Void ratio, $e_{D_r=50\%}$ [#]	Normal stress, σ_n (kPa)	Number of particles	
			Gravel	Rubber
0	0.534	30 kPa	4483	0
	0.516	60 kPa		
	0.511	100 kPa		
10	0.558	30 kPa	4109	754
	0.542	60 kPa		
	0.527	100 kPa		
25	0.595	30 kPa	3304	1537
	0.566	60 kPa		
	0.544	100 kPa		
40	0.601	30 kPa	2431	3063
	0.556	60 kPa		
	0.528	100 kPa		
70	0.677	30 kPa	1161	4192
	0.617	60 kPa		
	0.566	100 kPa		
100	0.782	30 kPa	0	5769
	0.681	60 kPa		
	0.598	100 kPa		

[#] Measured after the application of 30, 60 and 100 kPa normal stress (i.e., before shearing) in the direct shear tests.

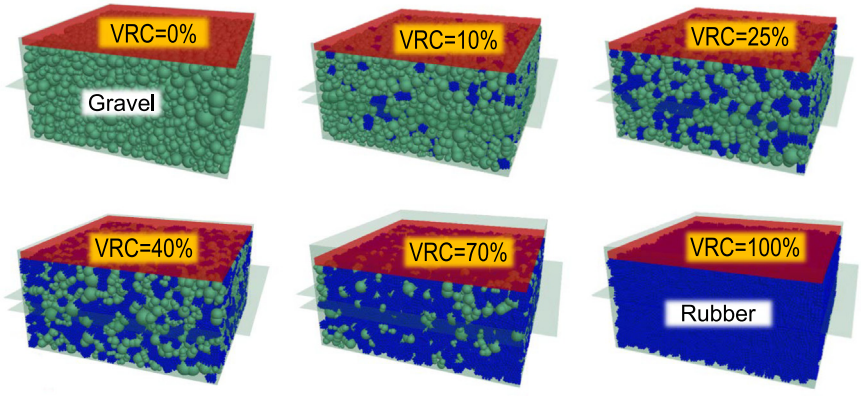

Fig. 9. GRM specimens and direct shear setup generated by the DEM4GRM model.

4.2. GRM micro-mechanical response

4.2.1. Fabric and force anisotropy

The methodology proposed by Rothenburg and Bathurst (1989) is used to quantify the fabric and force anisotropy in the GRM assembly during shearing with some required modifications that are in line with the latest research findings (e.g., Guo and Zhao, 2013). A curve fitting approach using second-order Fourier series yielded the following expressions that best describe the (polar) distribution of the different contact types considered in this study.

The expressions for fabric and normal force contact distributions are found to be similar to those originally proposed by Rothenburg and Bathurst (1989). The shape of the distribution of the contact vector – fabric can be approximated using the harmonic function:

$$E(\theta) = \frac{\{1 + a\ cos2(\theta - \theta_a)\}}{2\pi} \tag{7}$$

where a represents the magnitude or coefficient of anisotropy of the contact orientations and θ_a is the principal direction of this anisotropy.

Similarly, the contact normal force distribution is represented by:

$$\bar{f}_n(\theta) = \bar{f}_n^o\{1 + a_n cos2(\theta - \theta_n)\} \tag{8}$$

where $\bar{f}_n^o$ is the average contact normal force, a_n is the parameter describing the anisotropy of the contact normal force component, and θ_n is the direction of the maximum average normal forces.

On the other hand, the following expression is proposed and found to best approximate the tangential force distribution for the GRMs:

$$\bar{f}_t(\theta) = \bar{f}_t^o\{1 + a_t cos4(\theta - \theta_t)\} \tag{9}$$

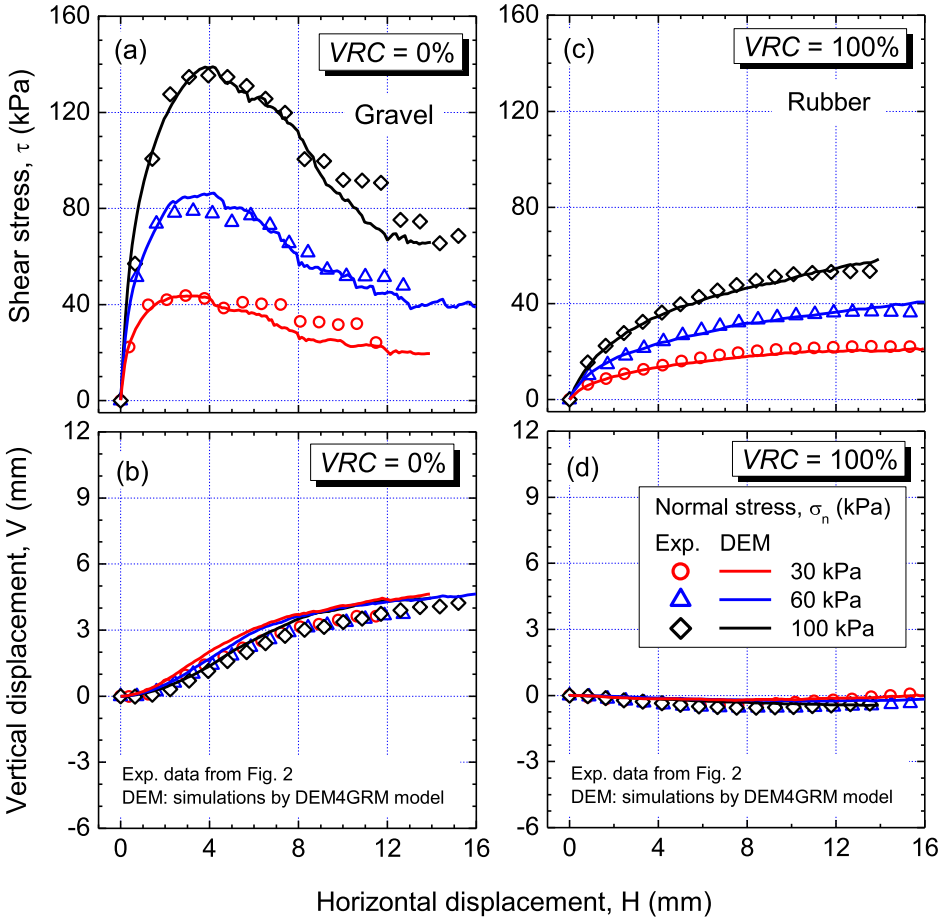

Fig. 10. DEM4GRM model simulations and their comparison with experimental test results at 30, 60 and 100 kPa normal stress: (a, b) gravel; and (c, d) granulated rubber specimens.

where $\bar{f}_t^o$ is the average contact shear force, a_t is the parameter describing the anisotropy of the contact tangential force component, and θ_t defines the direction of the peak contact shear force. Note that the latter expression differs from that of Rothenburg and Bathurst (1989), where the tangential force approaches zero between the peaks. This is, however, expected as in the earlier study by Rothenburg and Bathurst (1989) perfect spheres were considered, whereas in this study clumps are considered. The interlocking effects introduced by clumps give rise to 'background' tangential forces that are randomly orientated, and thus, the tangential forces do not diminish along orthogonal planes. The resultant tangential force distribution is akin to a superposition of an isotropic 'background' tangential forces that form a slightly different distribution to that observed by Rothenburg and Bathurst (1989).

Figs. 12–14 illustrate the comparison between the proposed fabric, normal force and tangential force anisotropy approximation functions and the observed DEM distributions at different horizontal displacement stages of the shearing process (i.e., 0 mm: end of the compression stage and before shearing; 0.2 mm: just after the beginning of shearing; 8.0 mm: approximately at the peak strength state; 14 mm: end of the test) for the case of $VRC = 10\%$ and 40% at 100 kPa normal stress. Very similar fabric and force anisotropy distributions are observed also for 30 kPa and 60 kPa normal stress.

Remarkably, independent of the VRC, the direction of normal force anisotropy (θ_n) starts at approximately 90° and typically reaches a value of 41-45° at large horizontal deformation (Fig. 15). Yet, its change during the shearing process is VRC depended. Specifically, for $VRC \leq 25\%$, the direction of normal anisotropy sharply decreases to a minimum value (the lowest being 28° for $VRC = 0\%$) and then increases with increasing shear displacement; on the other hand, for $VRC \geq 40\%$, it continuously decreases form 90° to 45° with increasing shear displacement. Similar trends are observed for 30 kPa and 60 kPa.

The variation during shearing at 100 kPa normal stress of the anisotropic coefficients a, a_n and a_t is shown in Fig. 16. In general, a, a_n and a_t values vary during the shearing process in a way that mostly resemble the macro-scale behavior (Figs. 10 and 11). It is important to mention that the plots attained for 30 kPa and 60 kPa are basically the same (therefore, they are not reported here; readers can refer to Chiaro et al. (2022) for details),

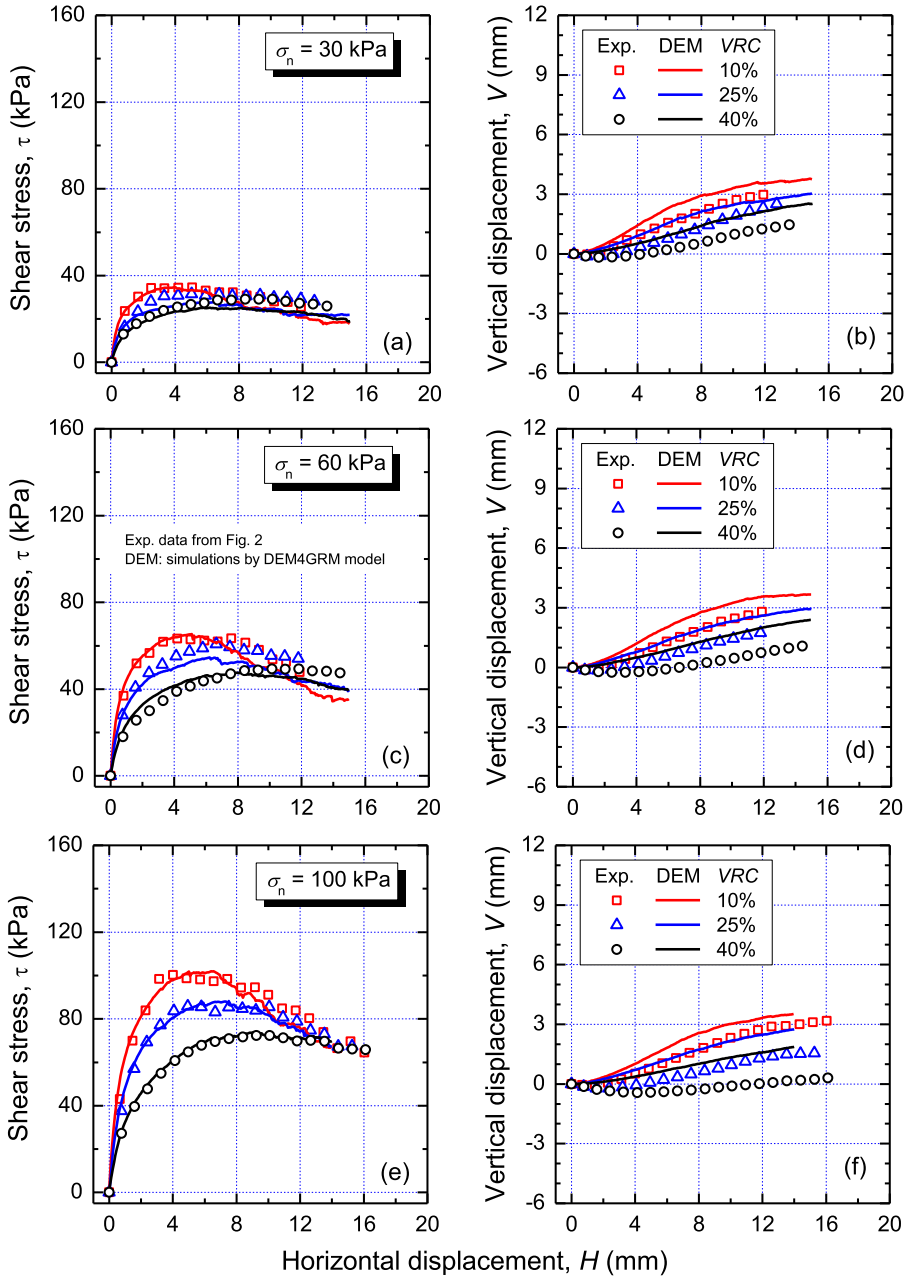

Fig. 11. Comparison between experimental and DEM direct shear responses of GRMs with various *VRC* at 30, 60 and 100 kPa normal stress.

indicating that a, a_n and a_t variation is significantly affected by *VRC* but not by the normal stress level.

The decrease in the fabric and force anisotropy (Fig. 16a, b, c) with increasing *VRC* can be attributed to the reduction in bulk friction of the assembly. Huang et al. (2014) investigated the effects of interparticle friction (μ) on the micro-mechanical responses at critical state and found that increasing interparticle friction resulted in higher degrees of anisotropy at critical state. Fig. 16(d) shows that the overall internal friction – found by dividing the total shear forces of all the contacts by the total normal forces – decreased with increasing *VRC*. Therefore, the addition of lower interparticle friction rubber particles reduces the bulk friction of the assembly, causing a reduction in the degree of anisotropy. Refer to Appendix A for solutions to the anisotropic parameters.

4.2.2. Strong-force network

It is well established that the contact network can be separated into two categories: the strong-force network, and the weak-force network (Radjai et al., 1998). The strong-force network consists of contact forces greater than the average force in the assembly, and represents the load-bearing force chains made of "primary" particles that is formed during shearing and is responsible for the fabric and force anisotropy observed (Guo and Zhao, 2013;

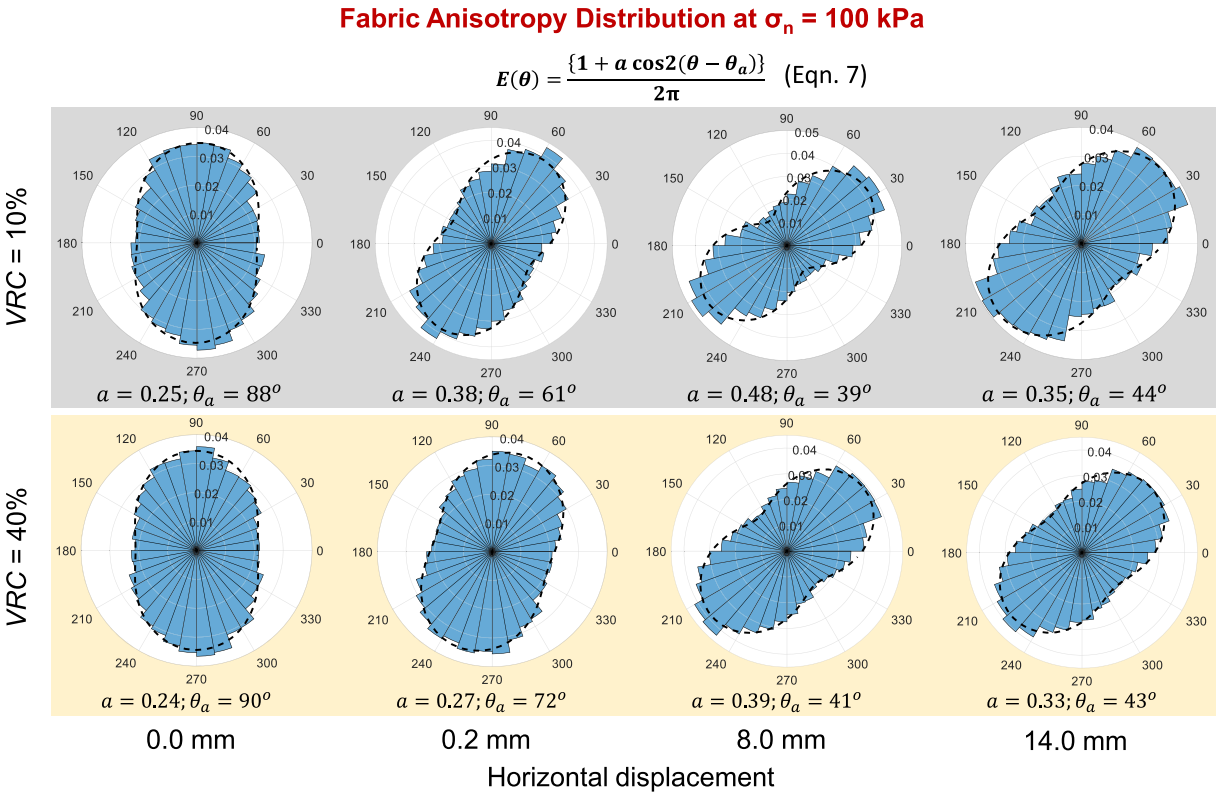

Fig. 12. Polar histograms of the fabric anisotropy distribution at different horizontal displacement levels ($VRC = 10\%$ and 40%; $\sigma_n = 100$ kPa). The dash lines ($--$) show the Fourier series approximation functions used in this study.

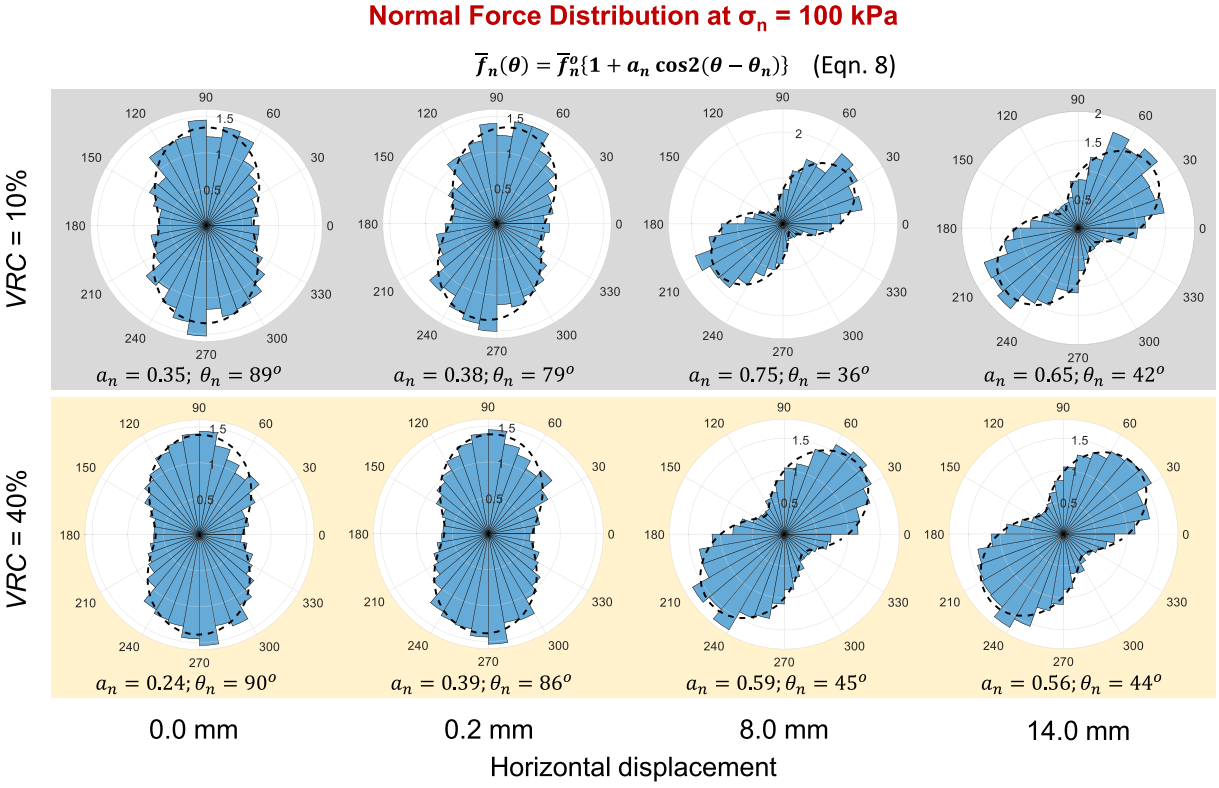

Fig. 13. Polar histograms of the normal force anisotropy distribution at different horizontal displacement levels ($VRC = 10\%$ and 40%; $\sigma_n = 100$ kPa). The dash lines ($--$) show the Fourier series approximation functions used in this study.

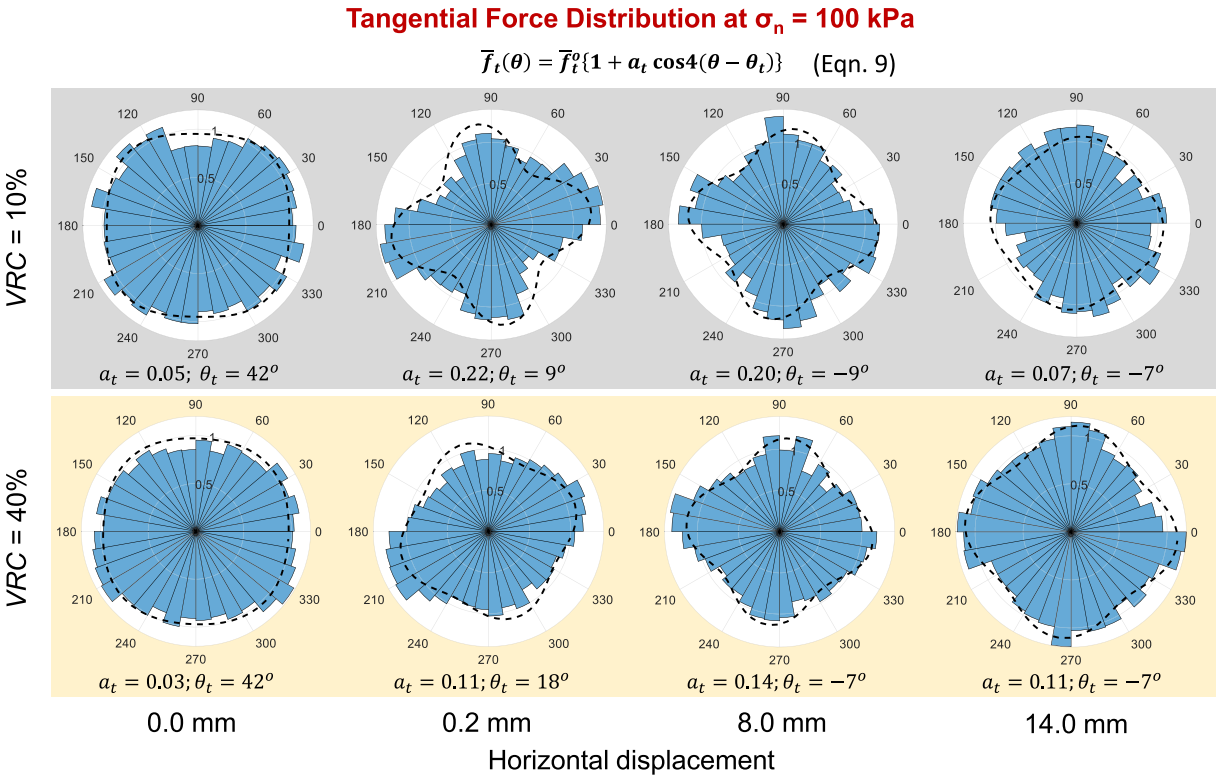

Fig. 14. Polar histograms of the tangential force anisotropy distribution at different horizontal displacement levels ($VRC = 10\%$ and 40%; $\sigma_n = 100$ kPa). The dash lines (– –) show the Fourier series approximation functions used in this study.

Huang et al., 2014; Lopera-Perez et al., 2017). The weak network is formed by "secondary" particles that do not carry load but rather prevent the buckling of the load-carrying chains (Radjai et al., 1998; Lee et al., 2007).

By computing the number of gravel-gravel (*g-g*), gravel-rubber (*g-r*) and rubber-rubber (*r-r*) contacts participating in the strong-force network, the plot shown in Fig. 17 is produced for 60 kPa normal stress. Although not reported here, identical trends are obtained for 30 kPa and 100 kPa normal stress.

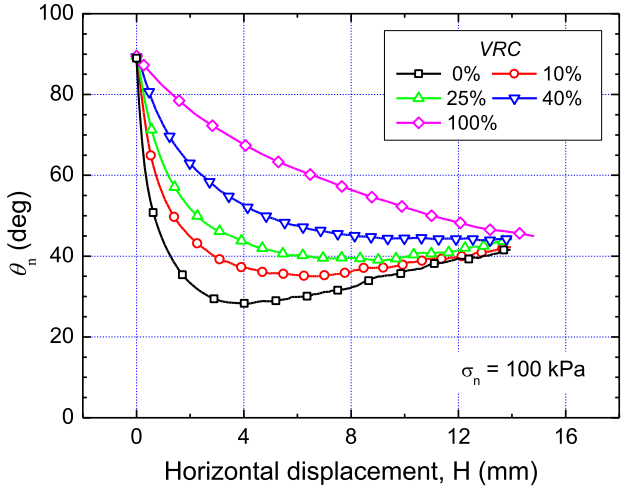

Fig. 15. Variation with *VRC* of GRM normal force orientation during sharing process at 100 kPa normal stress.

Fig. 17 shows that up to $VRC = 30\%$ the proportion of *r-r* contacts in the strong-force network is < 10%, while that of *g-g* contacts is > 50%. From 30% to 60% *VRC*, the proportion of *r-r* contacts increases significantly while that of *g-g* decreases rapidly. At $VRC = 40\%$, both these contact types carry an equal proportion (≈ 23–24%) of the load in the strong-force network. At this *VRC*, the strong-force chains are primarily transmitted via *g-r* contacts (≈ 53%), leading to a typical intermediate behavior where GRMs display a predominant dilative behavior during shearing, but the peak shear stress is much less pronounced as compared to that of pure gravel. Above $VRC = 60\%$, *r-r* contacts are the majority (> 50%) and form most of the strong-force chains (> 50%) in the assembly.

Relating the strong-force network results with some of the macro- and micro-responses discussed previously provides additional valuable insights. The variation in the bulk friction coefficient (μ) with increasing *VRC* (Fig. 16d) is very similar to the decrease in strong *g-g* contacts with increasing *VRC*. This indicates that the strong *g-g* contacts have a major influence on the shear strength of GRMs. When most of the force chains are transmitted through *g-g* contacts, it results in higher peak shear stresses and a greater degree of force anisotropy. This has also been observed by Lopera-Perez et al. (2017) for the case of SRMs.

4.2.3. Behavioral zones for GRMs

Independent of the level of normal stress, from the analyses of the strong-force network and the other micro-scale

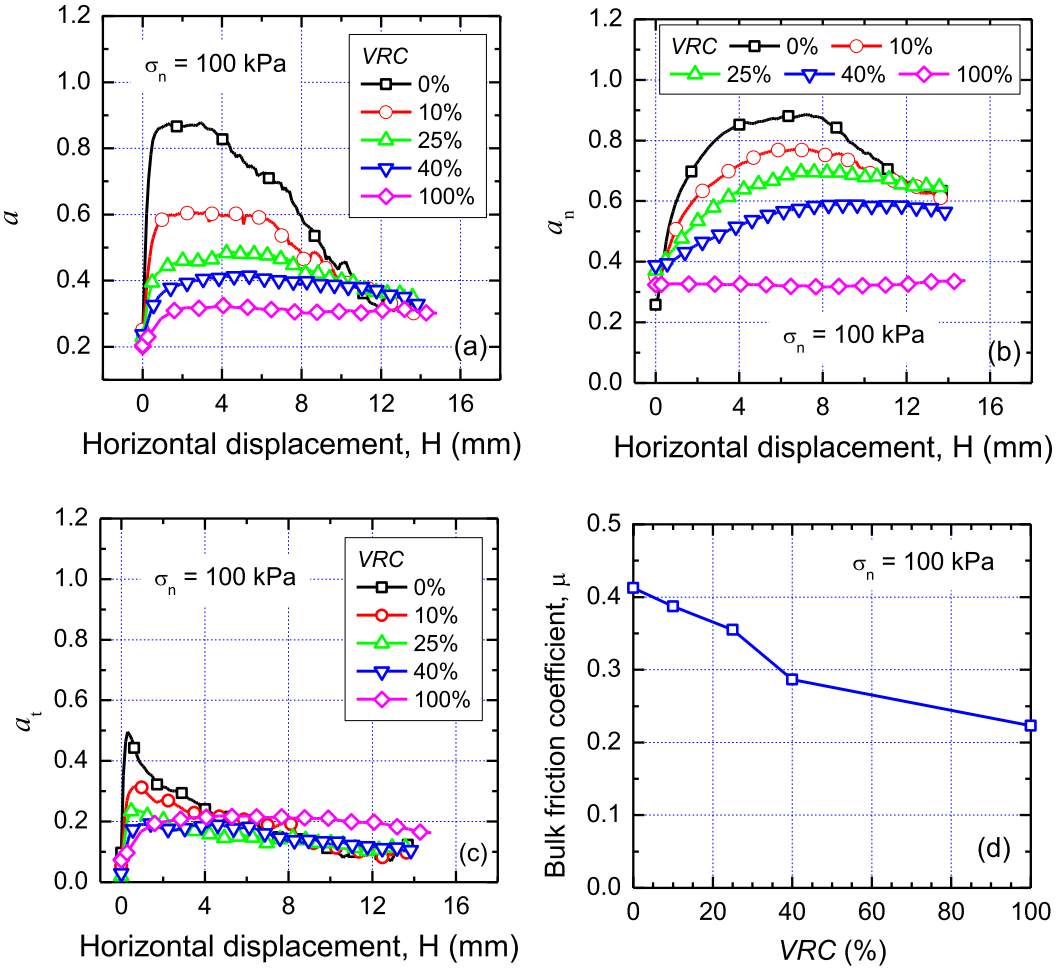

Fig. 16. Variation with *VRC* of GRM coefficients of anisotropy and bulk friction during sharing process at 100 kPa normal stress.

factors discussed previously, three behavioral zones are identified for GRMs (Fig. 17):

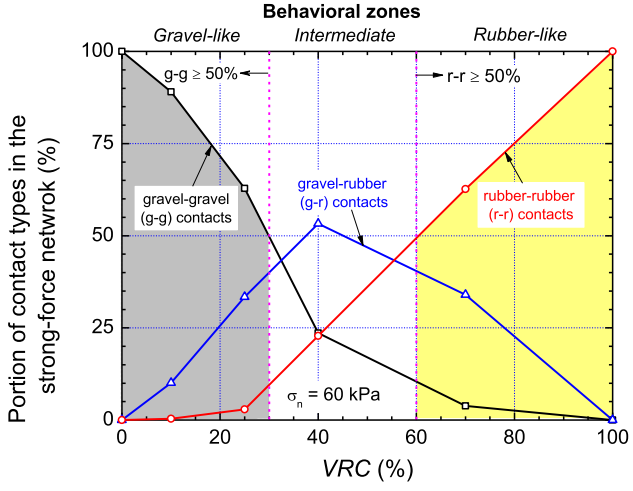

Fig. 17. Composition of the strong-force network and behavioral zones for GRMs in direct shear tests (numerical simulations by DEM4GRM model).

- *Rigid gravel-like behavior* for $VRC \leq 30\%$;
- *Intermediate (transitional) behavior* for $30\% < VRC < 60\%$; and
- *Soft rubber-like* for $VRC \geq 60\%$.

The proposed transition zone is in good agreement with the changes in the mechanical behavior identified experimentally for GRMs by the authors (e.g., Tasalloti et al., 2021a) and other researchers for GRMs (Pasha et al., 2020) and SRMs (Lee et al., 2007; Kim and Santamarina, 2008; Mashiri et al., 2015; Senetakis et al., 2012). Moreover, such results are also similar to DEM results reported by Asadi et al. (2018) for SRMs that had a similar particle size ratio as the GRMs considered in this study.

4.2.4. Compressive strain

The average compressive forces/strain in the bonds of the rubber particles increases with increasing *VRC* (Fig. 18). This correlates well with the observed macro- and micro-responses. As the *VRC* increases, more rubber particles participate in the strong-force network/load-bearing contacts (r-r and g-r) as indicated by Fig. 17. As more load is taken by the rubber particles, a significant

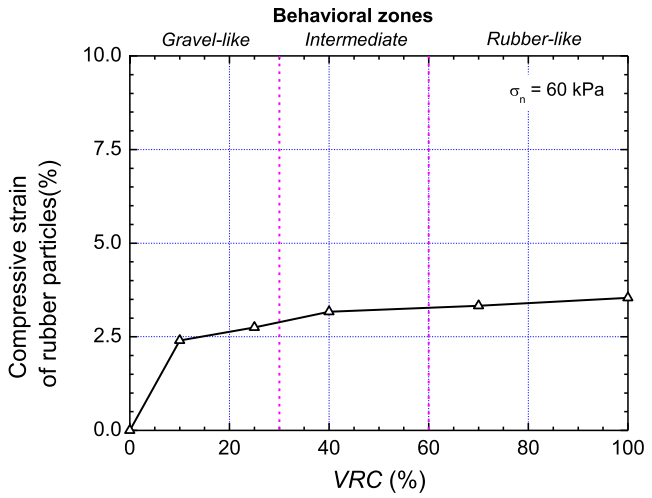

Fig. 18. Average compressive strain in the rubber particles at the end of shearing (numerical simulations by DEM4GRM model).

increase in the compressive strain within the rubber particles is developed, in turn causing a macro-scale more compressive behavior with increasing *VRC* as shown by the volumetric responses reported in Figs. 10 and 11. These findings highlight the important role of the strong-force chains in governing the strength and deformation characteristics of GRMs.

4.2.5. Discussion

GRMs are essentially binary granular materials consisting of rigid and soft particles of different sizes and shapes. As indicated by both experimental (e.g., Lee et al., 2007; Senetakis et al., 2012; Mashiri et al., 2015; Pasha et al., 2019; Tasalloti et al, 2021a, among others) and DEM studies (e.g., Lopera-Perez 2017a, 2017b), the packing density (i.e., void ratio) and mechanical behavior (i.e. compressibility and strength) of soil-rubber mixtures is significantly influenced by the inherent properties of the materials (i.e. size and shape), the proportion of large/small and soft/-rigid particles in the total volume of solids as well as the size ratio of large/small ($D_{50,large}/D_{50,small}$) and rigid/soft (i.e., aspect ratio, $AR = D_{50,Rubber}/D_{50,Gravel}$) particles and the stress level applied. To give an example, Table 4 provides a schematic summary of rubber-gravel interaction in mixtures with different *VRC* ranging from 0 to 100% and two aspect ratios (*AR*) of 0.27 and 0.67 based on experimental findings (Tasalloti et al., 2021a). The case of $AR = 0.67$ is the same of the GRMs investigated in this paper, and it is interesting to notice the agreement between the expected behavior based on skeleton material from macro-mechanical analyses and the behavioral zones established by the DEM investigations.

While in this study it is found that the stress level had negligible influence on the behavioral zone, indicating a

Table 4
Schematic summary of rubber-gravel interaction in mixtures with different *VRC* and aspect ratios (adopted from Tasalloti et al. (2021a) and republished with Elsevier permission).

Volumetric rubber content, *VRC* (%)	Skeleton material		Remarks
	$AR = 0.27$	$AR = 0.67$	
0	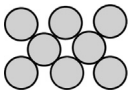	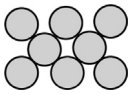	Rigid gravel skeleton
20	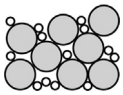	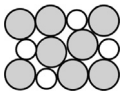	Gravel-controlled stiffness; rubber may prevent buckling of gravel columns; $AR = 0.27$: segregation if rubber can pass through gravel pores
40	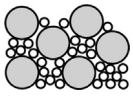	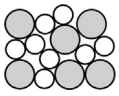	$AR = 0.27$: Transition mixture. Rubber separates gravel contacts at low pressures; gravel contacts may form at large pressures. $AR = 0.67$: Rubber forms percolating skeleton. There is gravel-gravel grain interaction
60	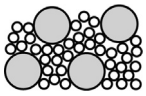	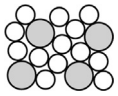	Gravel forms percolating skeleton. There is rubber-rubber particle interaction
80	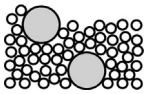	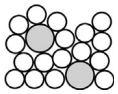	Rubber-controlled stiffness
100	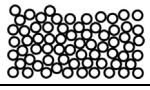	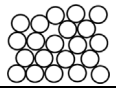	Soft rubber skeleton

similar load-transfer mechanism under different levels of normal stress, which in any case here is limited to 100 kPa, Table 4 suggests that it may not be the case when the same rounded gravel would be mixed with smaller rubber particles (e.g., $AR = 0.27$). Thus, to provide new and more comprehensive insights on the GRMs load-transfer mechanisms and associated behavioral zones, while accounting for the rubber size effects and normal stress level, more in-depth micro-mechanical investigations are required. Hence, the authors are planning to conduct additional DEM simulations using the DEM4GRM model presented in this paper pairing macro-scale experimental results for the rounded gravel used in this study (Tasalloti et at., 2021a; Chiaro et al., 2022) and a similar-size angular gravel (Chiaro et al., 2021) for $AR = 0.27$–0.67 that are already available.

5. Conclusions

In this paper, a newly developed 3-dimentional discrete element model, namely DEM4GRM, is presented and used to evaluate the micro-scale direct shear mechanical behavior of rigid-soft gravel-rubber mixtures (GRMs). Rigid gravel grains are modelled as simple multi-shape rigid clumps, while soft rubber particles are modeled by using deformable 35-ball body-centered-cubic clusters. The change of fabric, normal and tangential force anisotropy is then examined throughout the shearing process by means of novel micro-mechanical relationships valid for GRMs. Moreover, strong-force chains are scrutinized to identify the transition from rigid to soft granular skeleton and gain insights on the load transfer and deformation mechanisms of GRMs.

The following key conclusions can be drawn from this study:

- By using a single set of 16 model parameters (primarily experimentally derived), the proposed DEM4GRM model can accurately describe the macro-scale direct shear response of GRMs, from small to large horizontal displacement (over the full range of volumetric rubber content (VRC) and for different normal stress levels), and provide detailed information on the micro-scale mechanical behavior;
- The proposed 35-ball body-centered-cube clusters, used to model single rubber particles, make it possible to realistically account for particle-level rubber deformability and obtain accurate description of the macro-scale volumetric behavior of GRMs during the entire shearing process;
- The use of multi-shape clumps not only permits modeling rigid gravel grains while properly accounting for grain size and shape variability, but also introduces more realistic particle-to-particle interlocking effects that give rise to "background" randomly-orientated tangential forces, that otherwise are neglected when using idealized rigid spheres;
- Micro-mechanics analyses have shown that the development of the fabric and force anisotropy during shearing is closely related to the macro-scale shear strength of GRMs, and strongly depends on the VRC; moreover, the distribution of such micro-scale factors can be described by Fourier functions;
- Strong-force chains, responsible for the load-transfer and deformation mechanisms, appear to be primarily formed by gravel-gravel contacts up to $VRC = 30\%$, and by rubber-rubber contacts beyond $VRC = 60\%$. Alternatively, at $30\% < VRC < 60\%$, gravel-rubber contacts are dominant in the strong-force network;
- On the basis of the strong-force network characteristics, three behavioral zones are defined for GRMs: (1) *Rigid gravel-like behavior* for $VRC \leq 30\%$; (2) *Intermediate (transitional) behavior* for $30\% < VRC < 60\%$; and (3) *Soft rubber-like* for $VRC \geq 60\%$. This is consistent with the behavioral trends observed in the macro- and micro-mechanical responses.

This study has demonstrated the insightful observations that can be obtained from DEM investigations to inform and validate experimental studies or vice versa. The authors are planning to extend this study and consider GRMs with different aspect ratios and rounded/angular gravel particles (experimental data are already available and have been published by the authors elsewhere) as well as dynamic testing conditions to investigate the strain-dependent properties of GRMs (i.e., shear modulus degradation and damping ratio) from a micro-mechanical viewpoint. Future studies could also consider additional pairing grain-scale experiments on gravel-rubber interfaces to further calibrate the DEM4GRM model presented here.

Acknowledgment

The authors would like to acknowledge the research funds provided by the Ministry of Business, Innovation and Employment of New Zealand (MBIE Smart Ideas Endeavour Research Grant No. 56289). The IT logistics support provided by Olive Dalton (Systems Manager, UC) and Paul Strange (Special System Support, UC) is also greatly appreciated.

Appendix A. Determination of anisotropy coefficient and orientation

Most of the proposed contact distribution expressions take the form $[1 + \widehat{a}cos2\left(\theta - \widehat{\theta}_a\right)]$. Ignoring the constants used to normalise the data, a typical contact distribution is defined as.

$$\widehat{E}(\theta) = 1 + \widehat{a}cos2\left(\theta - \widehat{\theta}_a\right) \tag{A1}$$

where $\widehat{a}$ and $\widehat{\theta}_a$ are the anisotropy coefficient and direction of anisotropy of the considered contact type, respectively. As shown by Rothenburg and Bathurst (1989), the factors $\widehat{a}$ and $\widehat{\theta}_a$ can be determined using the following relationships:

$$\int_0^{2\pi}\left[1+\widehat{a}\cos 2\left(\theta-\widehat{\theta}_a\right)\right]\cos 2\theta\, d\theta = \widehat{a}\,\pi\cos 2\widehat{\theta}_a$$

$$\int_0^{2\pi}\widehat{E}(\theta)sin2\theta d\theta = \widehat{a}\pi sin2\widehat{\theta}_a \quad \text{(A3)}$$

where $\widehat{E}(\theta)$ is the portion of contacts within each interval which can be determined from the micromechanical contact data obtained from the PFC model. As this data is discrete, a numerical integration method (e.g. Trapezium Rule) is used to estimate the left-hand-side of Eqns. A2 and A3. Thus, allowing the (unknown) parameters $\widehat{a}$ and $\widehat{\theta}_a$ to be solved for. $\widehat{\theta}_a$ gives the major principal direction where $\widehat{a} > 0$, while $\widehat{a} < 0$ yields the minor principal direction.

Similarly, in this study, for the tangential distribution function that it is defined using the 4th harmonic term, the parameters $\widehat{a}$ and $\widehat{\theta}_a$ are solved for using the following relationships:

$$\int_0^{2\pi}\left[1+\widehat{a}\cos 4\left(\theta-\widehat{\theta}_a\right)\right]\cos 4\theta\, d\theta = \widehat{a}\,\pi\cos 4\widehat{\theta}_a$$

$$\int_0^{2\pi}\widehat{E}(\theta)sin4\theta d\theta = \widehat{a}\pi sin4\widehat{\theta}_a \quad \text{(A5)}$$

References

Anastasiadis, A., Senetakis, K., Pitilakis, K., 2012. Small-strain shear modulus and damping ratio of sand-rubber and gravel-rubber mixtures. Geotech. Geol. Eng. 30 (2), 363–382.

Asadi, M., Mahboubi, A., Thoeni, K., 2018. Discrete modeling of sand–tire mixture considering grain-scale deformability. Granul. Matter 20, 1–13.

ASTM D3080-11, 2011. Standard Test Method for Direct Shear Test of Soils Under Consolidated Drained Conditions. ASTM International, West Conshohocken, PA.

ASTM D4253-16, 2016. Standard Test Methods for Maximum Index Density and Unit Weight of Soils Using a Vibratory Table. ASTM International, West Conshohocken, PA.

ASTM D698-12, 2012. Standard Test Methods for Laboratory Compaction Characteristics of Soil Using Standard Effort (12,400 ft-lbf/ft3 (600 kN-m/m3)). ASTM International, West Conshohocken, PA.

Banasiak, L.J., Chiaro, G., Palermo, A., Granello, G., 2021. Environmental implications of the recycling of end-of-life tires in seismic-isolation foundation systems. In: Advances in Sustainable Construction and Resource Management, Lect. Notes Civ. Eng., vol. 144, pp. 43–52.

Chew, K., 2021. The mechanical behaviour of gravel-rubber mixtures: insights from DEM numerical investigations. MEng Thesis, University of Canterbury, p. 129.

Chiaro, G., Palermo, A., Granello, G., Tasalloti, A., Stratford, C., Banasiak, L.J., 2019. Eco-rubber seismic-isolation foundation systems: a cost-effective way to build resilience. In: Proc. of the 2019 Pacific Conf. Earthquake Eng., Auckland, New Zealand, p. 8.

Chiaro, G., Palermo, A., Granello, G., Tasalloti, A., Banasiak, L.J., 2021. Reuse of waste tires to develop eco-rubber seismic-isolation foundation systems. In: Advances in Sustainable Construction and Resource Management, Lect. Notes Civ. Eng., vol. 144, pp. 159–169.

Chiaro, G., Tasalloti, A., Banasiak, L., Palermo, A., Granello, G., Rees, S., 2020. Sustainable recycling of end-of-life tyres in civil (geotechnical) engineering applications: turning issues into opportunities in the New Zealand context. NZ Geomech. News 99, 38–47.

Chiaro, G., Tasalloti, A., Chew, K., Vinod, J.S., Allulakshmi, K., 2022. Macro- and micro-scale engineering response of rigid-soft gravel-rubber inclusions: insights from detailed laboratory and DEM numerical investigations. Lect. Notes Civ. Eng. 196, 11–27.

Coetzee, C.J., 2017. Review: calibration of the discrete element method. Powder Technol. 310, 104–142.

Cui, L., O'Sullivan, C., 2006. Exploring the macro- and micro-scale response of an idealised granular material in the direct shear apparatus. Geotechnique 56, 455–468.

Cundall, P.A., Strack, O.D.L., 1979. Discrete numerical model for granular assemblies. Geotechnique 29 (1), 47–67.

Dhanya, J.S., Boominathan, A., Banarjeee, S., 2018. Performance of geo-base isolation system with geogrid reinforcement. Int. J. Geomech. 19 (7), 04019073.

Dhanya, J.S., Boominathan, A., Banarjeee, S., 2020. Response of low-rise building with geotechnical seismic isolation system. Soil Dyn. Earthquake Eng. 136 106187.

Evans, T.M., Valdes, J.R., 2008. Sand-rubber mixtures: experiments and numerical simulations. Canadian Geotech. J. 45 (4), 588–595.

Garcia, F.E., Bray, J.D., 2019. Modeling the shear response of granular materials with discrete element assemblages of sphere-clusters. Comput. Geotech. 106, 99–107.

Gong, J., Liu, J., Cui, L., 2019a. Shear behaviours of granular mixtures of gravel-shaped coarse and spherical fine particles investigated via discrete element method. Powder Technol. 353, 178–194.

Gong, L., Nie, L., Xu, Y., Wang, H., Zhang, T., Du, C., Wang, Y., 2019b. Discrete element modelling of the mechanical behaviour of a sand-rubber mixture containing large rubber particles. Constr. Build. Mater. 205, 574–585.

González-Montellano, C., Fuentes, J.M., Ayuga-Téllez, E., Ayuga, F., 2012. Determination of the mechanical properties of maize grains and olives required for use in DEM simulations. J. Food Eng. 111, 553–562.

Guo, N., Zhao, J., 2013. The signature of shear-induced anisotropy in granular media. Comput. Geotech. 47, 1–15.

Hazarika, H., Pasha, S.M.K., Ishibashi, I., Yoshimoto, N., Kinoshita, T., Endo, S., Karmokar, A.K., Hitosugi, T., 2020. Tire-chip reinforced foundation as liquefaction countermeasure for residential buildings. Soils Found. 60 (2), 315–326.

Hernandez, E., Palermo, A., Granello, G., Chiaro, G., Banasiak, L., 2020. Eco-rubber seismic-isolation foundation systems, a sustainable solution for the New Zealand context. Struct. Eng. Int. 30 (2), 192–200.

Huang, X., Hanley, K.J., O'Sullivan, C., Kwok, C.Y., 2014. Exploring the influence of interparticle friction on critical state behaviour using DEM. Int. J. Numer. Anal. Methods Geomech. 38, 1276–1297.

Indraratna, B., Ngo, N.T., Rujikiatkamjorn, C., Vinod, J.S., 2014. Behavior of fresh and fouled railway ballast subjected to direct shear testing: discrete element simulation. Int. J. Geomech. 14, 34–44.

Itasca Consulting Group, 2018. Particle flow code in three dimensions PFC3D. Manual guide.

Kim, H.K., Santamarina, J.C., 2008. Sand–rubber mixtures (large rubber chips). Can. Geotech. J. 45 (10), 1457–1466.

Lee, J.S., Dodds, J., Santamarina, J.C., 2007. Behavior of rigid-soft particle mixtures. J. Mater. Civ. Eng. 19, 179–184.

Lopera-Perez, J.C., Kwok, C.Y., O'Sullivan, C., Huang, X., Hanley, K.J., 2016. Assessing the quasi-static conditions for shearing in granular media within the critical state soil mechanics framework. Soils Found. 56 (1), 152–159.

Lopera-Perez, J.C., Kwok, C.Y., Senetakis, K., 2017a. Investigation of the micro-mechanics of sand–rubber mixtures at very small strains. Geosynth. Int. 24, 30–44.

Lopera-Perez, J.C., Kwok, C.Y., Senetakis, K., 2017b. Micromechanical analyses of the effect of rubber size and content on sand–rubber mixtures at the critical state. Geotext. Geomembranes 45, 81–97.
Lopera-Perez, J.C., Kwok, C.Y., Senetakis, K., 2018. Effect of rubber content on the unstable behaviour of sand–rubber mixtures under static loading: a micro-mechanical study. Geotechnique 68 (7), 561–574.
Mashiri, M.S., Vinod, J.S., Sheikh, M.N., Tsang, H.-H., 2015. Shear strength and dilatancy behaviour of sand–tyre chip mixtures. Soils Found. 55 (3), 517–528.
Mindlin, R.D., Deresiewicz, H., 1953. Elastic spheres in contact under varying oblique forces. J. Appl. Mech. 20, 327–344.
Ministry for the Environment, 2015. Waste tyres economic research. Report 3, p. 87.
Morimoto, T., Otsubo, M., Koseki, J., 2021. Microscopic investigation into liquefaction resistance of pre-sheared sand: effects of particle shape and initial anisotropy. Soils Found. 61 (2), 335–351.
Ngo, N.T., Indraratna, B., Rujikiatkamjorn, C., 2014. DEM simulation of the behaviour of geogrid stabilised ballast fouled with coal. Comput. Geotech. 55, 224–231.
O'Sullivan, C., 2011. Particulate Discrete Element Modelling: A Geomechanics Perspective. Spon Press, Abingdon, p. 561.
Ostubo, M., O'Sullivan, C., 2018. Experimental and DEM assessment of the stress-dependency of surface roughness effects on shear modulus. Soils Found. 58 (3), 602–614.
Pasha, S.M.K., Hazarika, H., Yoshimoto, N., 2019. Physical and mechanical properties of gravel-tire chips mixture (GTCM). Geosynth. Int. 26, 92–110.
Paulick, M., Morgeneyer, M., Kwade, A., 2015. A new method for the determination of particle contact stiffness. Granul. Matter 17, 83–93.
Pistolas, G.A., Anastasiadis, A., Pitilakis, K., 2015. Dynamic properties of gravel – recycled rubber mixtures: resonant column and cyclic triaxial tests. Geotech. Eng. Infrastruct. Dev., 2613–2618
Pitilakis, D., Anastasiadis, A., Vratsikidis, A., Kapouniaris, A., Massimino, M.R., Abate, G., Corsico, S., 2021. Large-scale field testing of geotechnical seismic isolation of structures using gravel-rubber mixtures. Earthq. Eng. Struc. Dyn. 50, 2712–2731.
Potyondy, D.O., Cundall, P.A., 2004. A bonded-particle model for rock. Int. J. Rock Mech. Min. Sci. 41 (8), 1329–1364.
Radjai, F., Wolf, D.E., Jean, M., Moreau, J.J., 1998. Bimodal character of stress transmission in granular packings. Phys. Rev. Lett. 80, 61–64.
Ren, Z.L., Cheng, Y.P., Xu, X., 2020. A DEM method for simulating rubber tyres. Géotechnique Lett. 10, 73–79.
Rothenburg, L., Bathurst, R.J., 1989. Analytical study of induced anisotropy in idealized granular materials. Geotechnique 39, 601–614.
Salot, C., Gotteland, P., Villard, P., 2009. Influence of relative density on granular materials behaviour: DEM simulations of triaxial tests. Granul. Matter 11 (4), 221–236.
Senetakis, K., Coop, M.R., 2014. The development of a new micromechanical inter-particle loading apparatus. Geotech. Test. J. 37 (6), 1028–1039.
Senetakis, K., Anastasiadis, A., Pitilakis, K., 2012. Dynamic properties of dry sand/rubber (SRM) and gravel/rubber (GRM) mixtures in a wide range of shearing strain amplitudes. Soil Dyn. Earthquake Eng. 33 (1), 38–53.
Sitharam, T.G., Dinesh, S.V., Shimizu, N., 2002. Micromechanical modelling of monotonic drained and undrained shear behaviour of granular media using three-dimensional DEM. Int. J. Numer. Anal. Methods Geomech. 26, 1167–1189.
Sitharam, T.G., Vinod, J.S., Ravishankar, B.V., 2009. Post-liquefaction undrained monotonic behaviour of sands: experiments and DEM simulations. Géotechnique 59 (9), 739–749.
Tasalloti, A., Chiaro, G., Palermo, A., Banasiak, L.J., 2020. Effect of rubber crumbs volumetric content on the shear strength of gravelly soil in direct shear apparatus. ASCE Geotech. Spec. Publ. 319, 259–266.
Tasalloti, A., Chiaro, G., Banasaik, L., Palermo, A., 2021a. Experimental investigation of the mechanical behaviour of gravel-granulated tyre rubber mixtures. Constr. Build. Mater. 273 121749.
Tasalloti, A., Chiaro, G., Murali, A., Banasiak, L., 2021b. Physical and mechanical properties of granulated rubber mixed with granular soils – a literature review. Sustainability 13 (8), 4309.
Tasalloti, A., Chiaro, G., Murali, A., Banasiak, L., Palermo, A., Granello, G., 2021c. Recycling of end-of-life tires (ELTs) for sustainable geotechnical applications: a New Zealand perspective. Appl. Sci. 11 (17), 7824.
Tian, Y., Senetakis, K., 2022. On the contact problem of soft-rigid interfaces: incorporation of Mindlin-Deresiewicz and self-deformation concepts. Granul. Matter 24, 28.
Tian, Y., Kasyap, S.S., Senetakis, K., 2021. Influence of loading history and soil type on the normal contact behavior of natural sand grain-elastomer composite interfaces. Polymers 13, 1830. https://doi.org/10.3390/polym13111830.
Tsang, H.H., 2008. Seismic isolation by rubber–soil mixtures for developing countries. Earthquake Eng. Struct. Dyn. 37 (2), 283–303.
Tsang, H.H., Lo, S.H., Xu, X., Neaz Sheikh, M., 2012. Seismic isolation for low-to-medium-rise buildings using granulated rubber-soil mixtures: numerical study. Earthquake Earthquake Eng. Struct. Dyn. 41 (14), 2009–2024.
Tsang, H.H., Tran, D.P., Hung, W.Y., Pitilakis, K., Gad, E.F., 2021. Performance of geotechnical seismic isolation system using rubber-soil mixtures in centrifuge testing. Earthquake Eng. Struct. Dyn. 50 (5), 1271–1289.
Tsang, H.H., 2009. Geotechnical Seismic Isolation. Earthquake Engineering: New Research. In: Miura, T., Ikeda, Y. (Eds.), Nova Science Publishers, Inc., New York, U.S., pp. 55–87.
Tyrewise, 2020. Regulated product stewardship for end of life tyres, "Tyrewise 2.0". Updated Report, p. 261.
Wang, C., Deng, A., Taheri, A., 2018. Three-dimensional discrete element modeling of direct shear test for granular rubber-sand. Comput. Geotech. 97, 204–216.
Zhang, J., Chen, X., Zhang, J., Jitsangiam, P., Wang, X., 2020. DEM investigation of macro- and micro-mechanical properties of rigid-grain and soft-chip mixtures. Particuology 55, 128–139.
Zhang, M., Yang, Y., Zhang, H., Yu, H.S., 2019. DEM and experimental study of bi-directional simple shear. Granul. Matter 21, 1–13.